Chemical Science

ROYAL SOCIETY OF CHEMISTRY

EDGE ARTICLE

View Article Online
View Journal | View Issue

Cite this: *Chem. Sci.*, 2020, **11**, 1683

All publication charges for this article have been paid for by the Royal Society of Chemistry

Concerted proton-electron transfer oxidation of phenols and hydrocarbons by a high-valent nickel complex†

Katherine J. Fisher, Margalit L. Feuer, Hannah M. C. Lant, Brandon Q. Mercado, Robert H. Crabtree * and Gary W. Brudvig *

Received 3rd November 2019
Accepted 29th December 2019

DOI: 10.1039/c9sc05565g

rsc.li/chemical-science

The high-valent nickel(III) complex $Ni(pyalk)_2^+$ (**2**) was prepared by oxidation of a nickel(II) complex, $Ni(pyalk)_2$ (**1**) (pyalk = 2-pyridyl-2-propanoate). **2** and derivatives were fully characterized by mass spectrometry and X-ray crystallography. Electron paramagnetic resonance spectroscopy and X-ray photoelectron spectroscopy confirm that the oxidation is metal-centered. **2** was found to react with a variety of phenolic and hydrocarbon substrates. A linear correlation between the measured rate constant and the substrate bond dissociation enthalpy (BDE) was found for both phenolic and hydrocarbon substrates. Large H/D kinetic isotope effects were also observed for both sets of substrates. These results suggest that **2** reacts through concerted proton-electron transfer (CPET). Analysis of measured thermodynamic parameters allows us to calculate a bond dissociation free energy (BDFE) of ~91 kcal mol^{-1} for the O–H bond of the bound pyalk ligand. These findings may shed light onto CPET steps in oxidative catalysis and have implications for ligand design in catalytic systems.

Introduction

Reactions in which protons and electrons move in a single, concerted step (concerted proton-electron transfer, or CPET) play a significant role in many organic, inorganic, and bioinorganic catalytic systems. CPET at high-valent metal centers has been proposed or observed in the catalytic mechanisms ranging from enzymatic reactions[1,2] to water-oxidation catalysis[3,4] to organic synthesis.[5,6] In many of these systems, the proton and electron are transferred to a high-valent metal–oxo species; however, another strategy involves the transfer of the proton to the ligand scaffold instead. This approach is also relevant to some bioinorganic systems. For instance, in nickel superoxide dismutase (NiSOD), a CPET step is proposed to occur at a highly oxidized nickel(III) intermediate in which a coordinated thiol or amide moiety acts as a proton donor.[7–9]

Understanding the CPET reactivity of high-valent metal centers may give some insight into their reactivity in catalytic systems. In particular, understanding CPET steps in systems in which the proton is transferred to the ligand may provide insight into catalytic systems which do not or cannot go through metal–oxo intermediates, such as copper- or nickel-containing water-oxidation catalysts or NiSOD.

In our previous studies, we found that the strongly donating ligand 2-pyridinyl-2-propanoate (pyalk) can stabilize metal centers in high oxidation states, including Ir(V).[10] In addition, the pyalk alkoxide has been suggested to act as a proton shuttle in catalytic water oxidation.[11,12] We reasoned that a high-valent metal compound stabilized by the pyalk ligand was a good candidate for fast CPET. We now describe the preparation of a stable Ni(III) species capable of reacting with a variety of O–H and C–H bonds *via* CPET.

Results and discussion

Characterization of Ni^{3+}

We prepared **1**, a new square-planar nickel(II) complex with two pyalk ligands arranged in a *trans* orientation (Scheme 1), which was characterized by X-ray crystallography, ^1H NMR spectroscopy, and cyclic voltammetry (CV). The CV of **1** shows a reversible redox feature at 0.15 V *vs.* Fc/Fc^+, suggesting that oxidation generates a stable Ni(III) species (Fig. 1).

In CH_2Cl_2, **1** was treated with [NO][BF_4] or [NO][PF_6] (E^0 = 0.6 V *vs.* Fc/Fc^+) (Scheme 1). The solution immediately changed from light green to deep blue. UV-visible spectroscopy indicated the presence of two intense features in the absorption spectrum (λ_{max} = 340 nm and 610 nm, Fig. S1†). This change suggested the formation of an oxidized species. Such intense absorption features in the visible and NIR regions are consistent with the data from other Ni(III) compounds,[13]

Department of Chemistry, Yale University, New Haven, CT 06520, USA. E-mail: robert.crabtree@yale.edu; gary.brudvig@yale.edu

† Electronic supplementary information (ESI) available: Experimental details, supplementary figures, and crystallographic data. CCDC 1954011–1954013. For ESI and crystallographic data in CIF or other electronic format see DOI: 10.1039/c9sc05565g

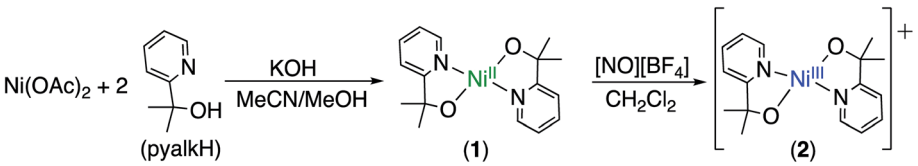

Scheme 1 Synthetic route for preparation of $Ni^{II}(pyalk)_2$ (**1**) and $Ni^{III}(pyalk)_2^+$ (**2**).

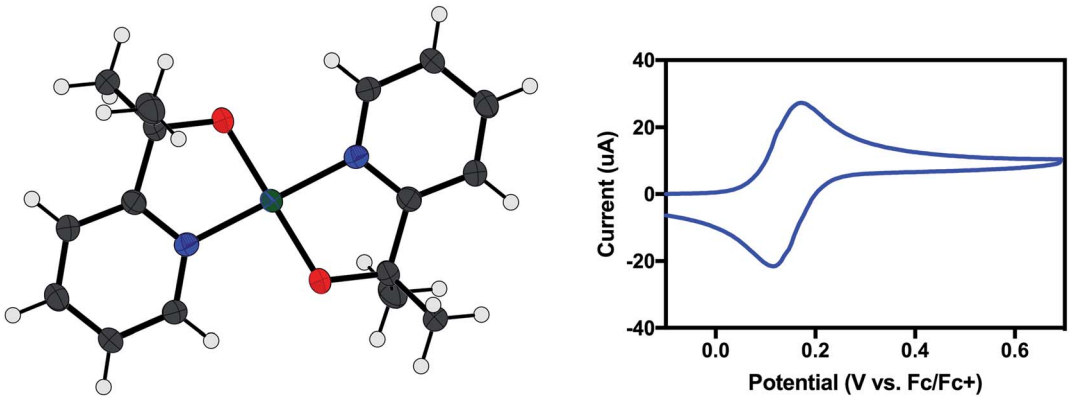

Fig. 1 (Left) X-ray crystal structure of $Ni(pyalk)_2$ (**1**). Atoms are shown at the 50% probability level (**1**). (Right) Cyclic voltammogram of **1** in MeCN. The reversible wave at 0.15 V *vs.* Fc/Fc^+ is assigned as a Ni(II/III) couple.

which led us to suspect that the Ni center had been oxidized. In addition, ^{1}H NMR of **2** gave a broad paramagnetic spectrum, in contrast to the diamagnetic spectrum of **1** (Fig. S3†). Measurement of the solution magnetic susceptibility by the Evans method[14] at room temperature gave a μ_{eff} of 1.87 for **2**, consistent with the presence of one unpaired electron, as expected for a square-planar Ni(III) compound.

Electron paramagnetic resonance (EPR) spectroscopy showed the presence of a single $S = \frac{1}{2}$ species (Fig. 2). A ligand centered oxidation would be expected to show an isotropic signal near $g = 2.0$. However, the observed rhombic spectrum had g values of $g_x = 2.077$, $g_y = 2.091$, $g_z = 2.274$ (Fig. 2, left). These g values, as well as $g_{ave} = 2.145$, are consistent with a low-spin square-planar d^7 Ni(III) complex.[15]

As demonstrated for a variety of iridium complexes,[16–19] X-ray photoelectron spectroscopy (XPS) provides another method for identifying a metal-centered oxidation. For metal-centered redox events with no change to the ligand set, the binding energy is expected to increase with oxidation state. Between **1** and **2**, the Ni 2p binding energy increases by 1.4 eV, consistent with a metal-centered oxidation from Ni(II) to Ni(III) (Fig. 2, right).

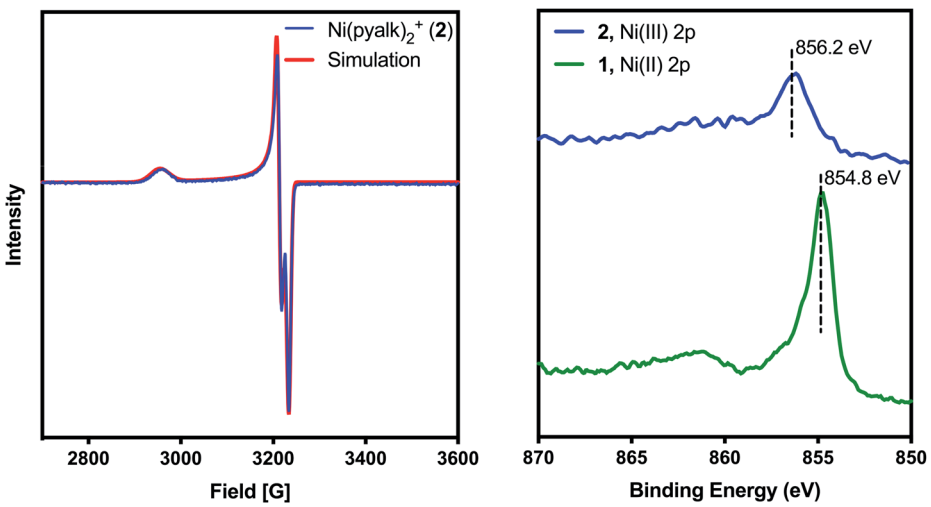

Fig. 2 (Left) Experimental (blue) and simulated (red) EPR spectra of **2** taken in CH_2Cl_2/toluene at 77 K. (Right) XPS spectrum of **2** (top) and **1** (bottom). The ~1 eV shift is consistent with a one-electron oxidation of the nickel center.

Electrospray ionization (ESI) mass spectrometry confirmed the molecular formula of **2**. A solution of **2** in CH_2Cl_2 gave a peak at $m/z = 330.09$ with the expected isotopic pattern for nickel (Fig. S2a†). A mass spectrum of the parent compound, **1**, was also taken, which showed a peak at $m/z = 331.09$ (Fig. S2b†), corresponding to [**1** + H^+]. Despite having the same elemental formula, **1** is uncharged, and thus is observed as the positively charged protonated species, whereas **2** bears a positive charge already, and so is observed without any associated ions. This result confirms that **2** is the one-electron oxidation product of **1**. The ESI mass spectrum of **2** does show a small signal at $m/z = 331.09$, which may indicate that some reduction of **2** occurs during the mass spectral analysis or over time in CH_2Cl_2.

Despite our best efforts, we were unable to obtain a crystal structure of **2**. While attempting to use pyridine as a co-solvent for crystallization, however, we observed that the solution changed from deep blue to bright orange (λ_{max} = 420 nm, Fig. S1†). Crystals of this new complex, **3**, were successfully grown from CH_2Cl_2/pentanes (Fig. 3, left). **3** proved to be an octahedral complex, with two equatorial pyalk ligands and two axial pyridines. **3** contains a PF_6^- anion, and a comparison of Ni–O bond lengths (Table S3†) indicates that the alkoxide arms of the pyalk ligands on **3** remain deprotonated, suggesting that **3** remains in the Ni(III) oxidation state. The EPR spectrum of **3** (Fig. 3, right) exhibits an axial signal with $g_x = 2.202$, $g_y = 2.163$, and $g_z = 2.030$. A five-line hyperfine pattern is observed on the g_z turning point, indicating coupling of the unpaired electron to the pyridyl nitrogens.[20] We found that the pyridine ligands do not remain bound in solution unless excess pyridine is present; when crystals of **3** were dissolved in CH_2Cl_2, **3** immediately reverted to **2**, as monitored by UV-visible spectroscopy (Fig. S1†). Upon addition of excess pyridine, the absorbance spectrum of **3** was re-established.

Remarkably, **2** and **3** are stable at room temperature, both as solids and in solution; this is rare for Ni(III) compounds, which tend to be stable only between −80 °C and −20 °C.[13,21,22]

Oxidation of phenols

With the oxidation state of **2** established, we sought to test its oxidative reactivity. We had shown in previous studies that the pyalk ligand could be reversibly protonated while coordinated to first row transition metals;[23] therefore, we hypothesized that **2** could undergo proton-coupled electron transfer (PCET) through the reaction proposed in Scheme 2.

To test **2** for PCET reactivity, **2** was treated with 100 equivalents of 2,4,6-tri-*tert*-butylphenol (TTBP), a common substrate for PCET reactions. When the colorless solution of TTBP was added to the deep blue solution of **2** in CH_2Cl_2, the color changed immediately to bright blue. The appearance of the characteristic peaks at 383 nm and 400 nm in the absorbance spectrum of this solution (Fig. 4) indicated that the tri-*tert*-butylphenoxyl radical had been formed, causing the color change,[24] and the disappearance of the features at 340 nm and 610 nm indicated that **2** had been consumed. In a similar reaction between **2** and 2,6-di-*tert*-butyl-phenol (DTBP), the radical coupling product 3,3′,5,5′-tetra-*tert*-butyl-[1,1′-bi(cyclohexylidene)]-2,2′,5,5′-tetraene-4,4′-dione was detected by gas chromatography-mass spectrometry (GC-MS, Fig. S4†). These results suggested that a PCET process was occurring.

For reactions of highly oxidized metal species with phenols, proton transfer followed by electron transfer (PT–ET), electron transfer followed by proton transfer (ET–PT), and concerted

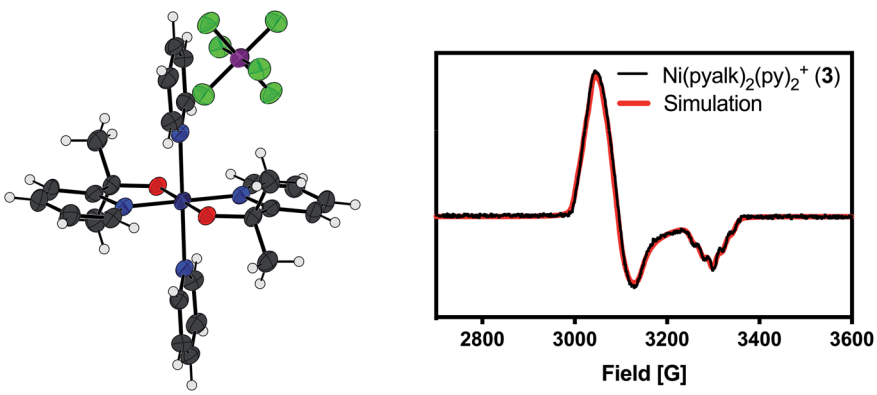

Fig. 3 (Left) X-ray crystal structure of **3**. Atoms are shown at the 50% probability level. A non-coordinated pyridine has been omitted for clarity. (Right) Experimental (black) and simulated (red) EPR spectra of **3** in CH_2Cl_2/pyridine at −80 °C.

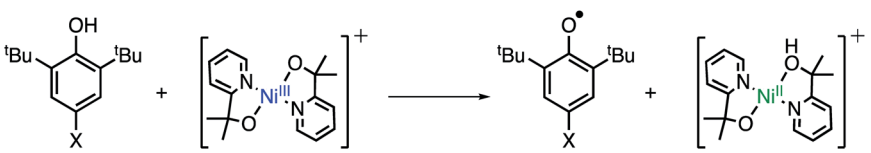

Scheme 2 Proposed PCET pathway for oxidation of phenols.

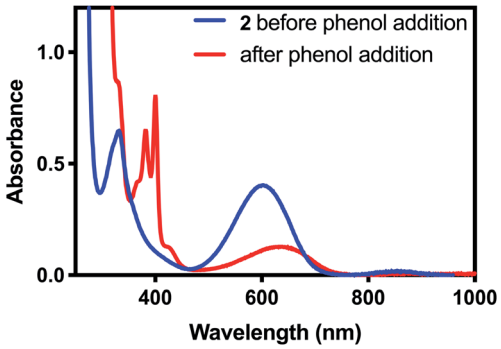

Fig. 4 UV-visible spectrum of **2** before (blue) and after (red) addition of excess tri-*tert*-butylphenol. The red trace is consistent with the published UV-visible spectrum of the tri-*tert*-butylphenoxyl radical.[24]

proton-electron transfer (CPET)/hydrogen atom transfer (HAT) mechanisms have all been observed.[25–27] Analysis of kinetic measurements can be used to differentiate between these mechanisms. Therefore, the kinetics of the reaction of **2** with a series of *para*-substituted 2,6-di-*t*-butylphenols (4-X-2,6-DTBP) was studied by stopped-flow spectrophotometry in order to further investigate the mechanism of oxidation by **2**. For these reactions, excess substrate was used to ensure pseudo-first order conditions (10–100 equivalents 4-X-2,6-DTBP). Representative UV-visible spectra as a function of time can be found in Fig. 5 and representative time traces can be found in Fig. S5 and S6.† Reactions with all substrates under these conditions fit well to a single exponential decay at a single wavelength (λ = 610 nm), for which global analysis gave k_{obs} values. Plots of k_{obs} *vs.* initial substrate concentration displayed a linear dependence (Fig. S7–S13†), allowing us to determine the second-order rate constant (k_2) for each substrate (Table S1†).

Measured k_2 values were plotted against the Hammett parameter σ_p^+ (Fig. 6, left). The σ_p^+ constant was chosen rather than σ_p because σ_p^+ is suggested to more accurately represent the electronic structure of the transition state for CPET from phenols[28] and a strong negative correlation between σ_p^+ and reaction rate is well known for this class of reactions.[29] Hammett

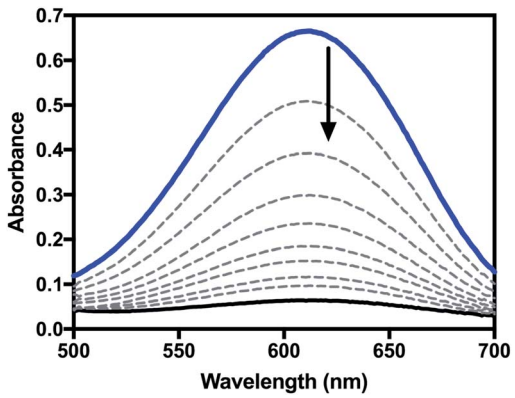

Fig. 5 Representative UV-visible spectra as a function of time for the reaction of **2** with 4-X-2,6-DTBP in CH_2Cl_2.

analysis showed that k_2 decreases with the electron-withdrawing capabilities of the *para*-substituent of the substrate ($\rho = -2.19$). This result is inconsistent with a rate-limiting proton transfer followed by electron transfer (PT–ET) mechanism, which would show a positive linear correlation in the Hammett plot.[30] The observed strong negative association is consistent with the formation of the electron deficient phenoxyl radical intermediate.[31,32] These results suggest a CPET mechanism for the reaction of 4-X-2,6-DTBP substrates with **2**. Similarly, the plot of log(k_2) *vs.* BDE_{O-H} of the phenol substrates also demonstrated a strong linear correlation (Fig. 6, right).[33] In contrast, the plots of k_2 *vs.* substrate pK_a or $E_{1/2}$ showed a much poorer correlation (Fig. S14†). This linear dependence also suggests a CPET mechanism and is consistent with similar plots constructed for other metal-based oxidants.[21,34,35] It should be noted that this mechanism could also be described as hydrogen atom transfer (HAT), which also operates through a concerted mechanism, and is frequently referred to as such in the literature.[36]

H/D kinetic isotope effects (k_2(H)/k_2(D), KIE) were also used to differentiate between the possible mechanisms. When the phenolic proton of 2,6-DTBP was replaced with a deuterium atom, the measured k_2 value decreased dramatically, and a KIE of ~4 was calculated (Fig. 7). A primary KIE of this magnitude implies that the cleavage of an O–H bond occurs in the rate-determining step, ruling out pathways involving rate-limiting electron transfer. This value for the KIE is also in good agreement with KIEs reported for the reaction of other metal-based oxidants with 2,6-DTBP that react *via* CPET.[22,31]

It should be noted that pK_a and BDE values used in our analysis were measured in dimethylsulfoxide (DMSO) rather than CH_2Cl_2, due to the lack of an absolute pK_a scale in CH_2Cl_2.[37] The general linear trend, however, is expected to remain the same regardless of solvent, as relative BDEs and BDFEs (bond dissociation free energies) do not change significantly with solvent. To test this assumption, the BDFEs in CH_2Cl_2 of several phenol substrates were estimated by converting from DMSO values using Abraham's empirical model.[38–40] Calculating BDFEs in this manner relies on a number of assumptions, which are discussed in more detail in the ESI (p. S20†), so the BDFE values should be treated as estimates only. Even so, we still see a strong linear correlation between log(k_2) and $BDFE_{CH_2Cl_2}$ (Fig. S15†). In a similar fashion, we also used Ingold's kinetic solvent effect relationship to calculate the expected rate constants in DMSO,[41] which we then plotted against known BDFEs and BDEs measured in DMSO (Fig. S16†). Once again, we saw a strong linear correlation, further supporting our conclusion of a CPET mechanism.

Oxidation of hydrocarbons

To further probe its CPET reactivity, **2** was also treated with a number of hydrocarbon substrates. Initial reactions of **2** with 1,4-cyclohexadiene and 9,10-dihydroanthracene produced the expected products of benzene and anthracene, as determined by gas chromatography and ^{1}H-NMR (Fig. S17a†). To determine the extent of reactivity of **2** with hydrocarbons, **2** was treated with a number of substrates having a range of C–H bond strengths.

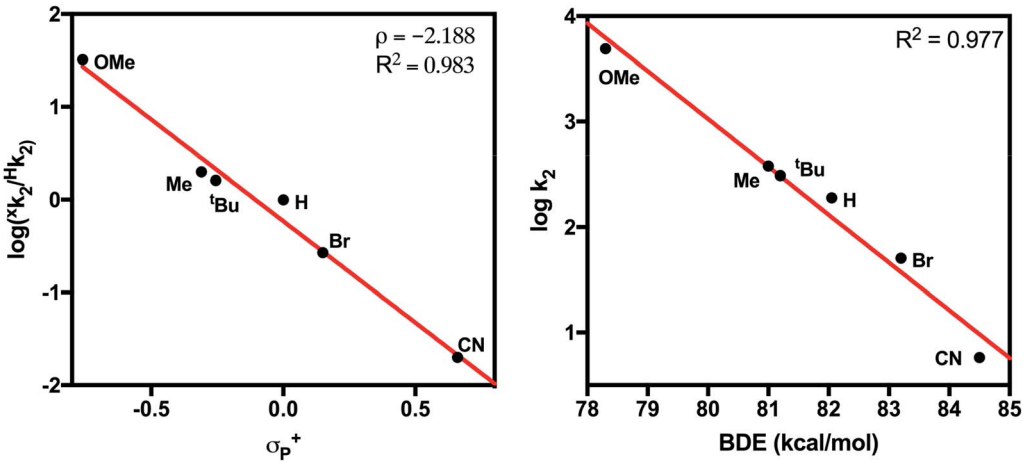

Fig. 6 (Left) Hammett plot for the reaction of **2** with 4-X-2,6-DTBP substrates. (Right) Plot of log(k_2) *vs.* BDE for 4-X-2,6-DTBP substrates.

As with phenols, the reactions were monitored by stopped-flow UV-visible spectroscopy or by UV-visible spectroscopy for slowly reacting substrates. All reactions were carried out under pseudo-first order conditions (10–100 equivalents of substrate). Reactions with all substrates under these conditions gave a good fit to a single exponential decay at a single wavelength ($\lambda = 610$ nm), except for reactions with THF, and global analysis was used to find k_{obs} values. For reactions with THF, the method of initial rates was used to find k_{obs} values. Plots of k_{obs} *vs.* substrate concentration gave good linear fits for all substrates, and the slopes of these fits were used to extract k_2 values for each substrate (Fig. S19–S25†). When appropriate, the data were statistically corrected to account for the number of hydrogen atoms susceptible to oxidation. For kinetic analysis of multi-proton/multi-electron reactions, such as the oxidation of 9,10-dihydroanthracene to anthracene (Fig. S17b†), the first concerted proton-electron transfer step was considered to be the rate-determining step, since the resulting radical species tend to have significantly lower BDEs than the parent compounds.[38,42,43]

2 was found to react with hydrocarbons with C–H bond strengths that ranged from 77–92 kcal mol^{-1}. For substrates with low C–H bond strengths, **2** reacted at appreciable rates – log k_2 values of 0.89 and 0.74 were found for reactions of **2** with 1,4-cyclohexadiene and dihydroanthracene (DHA), respectively. A plot of log(k_2) *vs.* C–H BDE showed a strong linear correlation (Fig. 8). In contrast, plots of log(k_2) *vs.* $E^0_{1/2}$ or pK_a showed a very poor correlation (Fig. S26†). This result strongly suggests a CPET mechanism for hydrocarbon oxidation.

To further investigate the mechanism, dihydroanthracene-d_4 was prepared, and an H/D kinetic isotope effect was measured. A large H/D KIE of ~11 was observed, indicating the involvement of a proton in the rate-determining step (Fig. S27†). This result, in combination with the linear correlation between log(k_2) and C–H bond strength, further supports our assignment of a CPET mechanism.

Thermodynamic analysis

We sought to identify the nickel-containing products of the reaction of **2** with phenol and hydrocarbon substrates. Based on our results suggesting that a CPET mechanism was at play, we

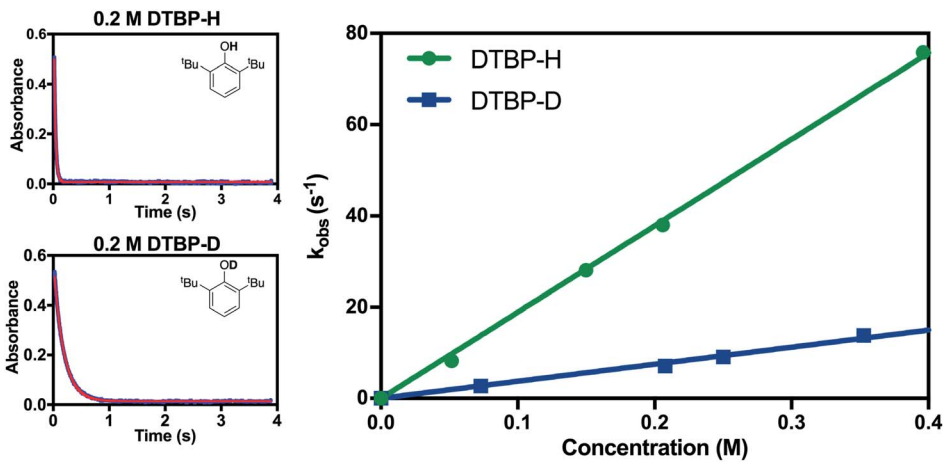

Fig. 7 (Left) Representative time trace of the absorbance at $\lambda = 610$ nm for the reaction of **2** with 2-6-DTBP-H (top) and 2,6-DTBP-D (bottom). (Right) Plot of k_{obs} *vs.* concentration for 2,6-DTBP-H and 2,6-DTBP-D substrates.

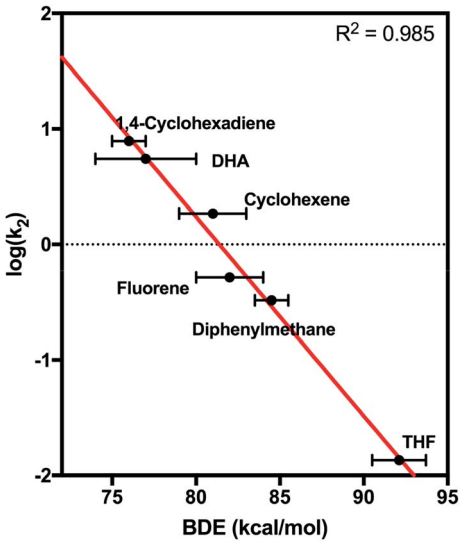

Fig. 8 Plot of log(k_2) *vs.* bond dissociation energy for the reaction of **2** with hydrocarbon substrates.

suspected that the nickel center was being reduced and that the pyalk ligand was accepting a proton and transforming the alkoxide ligand to an alcohol, resulting in the formation $[Ni(pyalk)(pyalkH)]^+$. The ^{1}H NMR spectrum of reaction products of **2** with 2,6-DTBP, however, showed only the presence of the fully deprotonated **1** in solution. A blue precipitate was also identified. This precipitate was dissolved in water and extracted into CH_2Cl_2 using $NaBAr^F$ (BAr^F = $[B[3,5\text{-}(CF_3)_2C_6H_3]_4]^-$). ^{1}H NMR analysis of the resulting product indicated the presence of $[Ni(pyalkH)_2][2(BAr^F)]$ (**4**) (Fig. 9a and S28†). This result suggests that, once the nickel metal center has been reduced, the pyalkH proton is labile enough to rearrange. Attempts to crystallize **4** were unsuccessful; however, when treating $Ni(OAc)_2$ with the pyalkH ligand, $Ni(pyalkH)_2(OAc)_2$ (**5**) was crystallized, demonstrating the binding of the pyalkH ligand to a nickel center (Fig. 9).

With the reaction products more fully understood, we constructed the square scheme in Scheme 3 to determine the thermodynamics of the reaction. The pK_a for the first deprotonation of the pyalk ligand of **4** (pK_{a1}, Fig. S29†) was estimated spectroscopically to be ~25 in MeCN using data from the deprotonation of **4** to **1**. Using this value, along with the

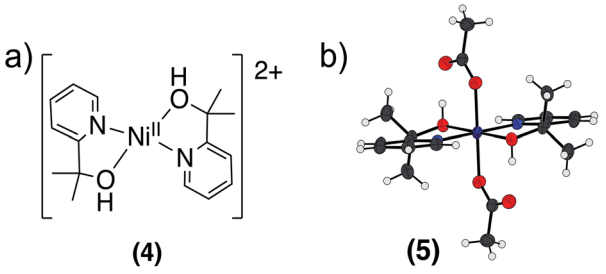

Fig. 9 (a) Structure of $[Ni(pyalkH)_2]^{2+}$ (**4**). (b) X-ray crystal structure of $Ni(pyalkH)_2(OAc)_2$ (**5**). Atoms are shown at the 50% probability level.

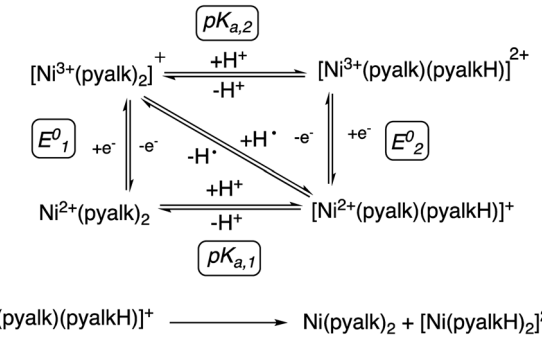

Scheme 3 Thermochemical square scheme for stepwise *vs.* concerted proton and electron transfer to the complexes described in this work. The lower equation shows the proposed proton exchange, explaining the observed products of reactions of **2** with substrates.

$E^0_{1/2}$ value of 0.15 V *vs.* Fc/Fc^+ in MeCN, we were able to determine a BDFE for the bound pyalk O–H bond of ~91 kcal mol^{-1} in MeCN using the square scheme shown in Scheme 3 and the following relationship:[38]

$$\mathrm{BDFE} = 13.7\mathrm{p}K_a + 23.06E^0 + C_{G,sol} \quad (1)$$

It is generally considered more appropriate to use BDFEs to describe the thermodynamics of PCET by transition metal complexes due to non-negligible entropic contributions.[38] However, many reported high-valent metal–oxo or metal–hydroxo oxidants report only the BDE of the O–H bond formed upon the reaction with substrate. Therefore, in order to facilitate a comparison between **2** and reported high-valent CPET/HAT reagents, the BDE of the pyalk O–H bond was also calculated. The BDE of the pyalk O–H bond for the CPET product of **2** was calculated using same thermochemical parameters described above and the following equation:

$$\mathrm{BDE} = 13.7\mathrm{p}K_a + 23.06E^0 + C_{H,sol} \quad (2)$$

For **2**, a BDE of ~94 kcal mol^{-1} in MeCN was calculated. This can be compared with a value of 105 kcal mol^{-1} for *t*BuO–H,[44]

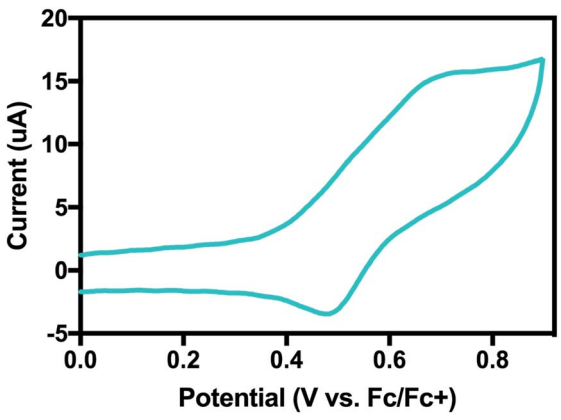

Fig. 10 Cyclic voltammogram of **4** in MeCN. The quasi-reversible couple at E^0 = 0.58 V *vs.* Fc/Fc^+ is assigned as a Ni(II/III) couple.

Table 1 Thermodynamic and kinetic parameters of high-valent metal compounds capable of performing CPET with hydrocarbon substrates

Compound	E_1^0 (V *vs.* Fc/Fc$^+$)	BDE (kcal mol^{-1})	log(k_2) DHA[a,b]	log(k_2) TTBP[a,b]	Ref.
$[Ni^{III}(pyalk)_2]^+$ (**2**)	0.15	94	0.74	2.48	This work
$Ni^{III}(^{Me}pyN_2)(ONO_2)$[f]	0.43	—	0.91		21
$Ni^{III}(^{Me}pyN_2)(Cl)$[f]	0.56	—	—	0.394[d]	22
$[(MeAN)Cu^{III}(\mu\text{-}O_2)Ni^{III}(^{Me}Nacnac)]^+$[g]	—	—	—	−0.82	45
$[Mn^{III}(H_3buea)(O)]^{2-}$[h]	−2.0	77	−0.53	—	25
$[Mn^{IV}(H_3buea)(O)]^-$[h]	−1.0	89	−1.59	—	25
$[Fe^{III}(PY5)(OCH_3)]^{2+}$[i]	0.73	84	−2.25	−0.22[e]	46
$Cu^{III}(^{iPr}pyN_2)(OH)$[j]	−0.074	90	2.27	—	34
$Ru^{IV}(bpy)_2(py)(O)$	0.48[c]	84	2.09	—	35, 47, and 48

[a] k_2 = second-order rate constant for reaction with the designated substrate, measured at 25 °C unless otherwise noted. [b] DHA = 9,10-diyhdroanthracene, TTBP = tri-*tert*-butylphenol (4-*t*Bu-2,6-DTPB). [c] *Vs.* SCE. [d] Measured at −40 °C. [e] Measured at −50 °C. [f] $^{Me}pyN_2$ = *N*,*N*′-(2,6-dimethylphenyl)-2,6-pyridinedicarboxamide. [g] MeAN = *N*,*N*,*N*′,*N*′,*N*′-pentamethyl-dipropylenetriamine and ^{Me}Nacnac = $[HC(CMeNC_6H_3(^iPr)_2)_2]$. [h] H_3buea = tris[(*N*′-*tert*-butylureaylato)-*N*-ethylene]amine. [i] PY5 = 2,6-bis(bis(2-pyridyl)methoxymethane)pyridine. [j] $^{iPr}pyN_2$ = *N*,*N*′-bis(2,6-diisopropylphenyl)-2,6-pyridinedicarboxamide.

taken as a model compound for free pyalkH, suggesting a modest O–H bond weakening on binding.

By cyclic voltammetry, **4** also showed a quasi-reversible redox feature in MeCN at $E^0_{1/2}$ = 0.58 V *vs.* Fc/Fc$^+$ (Fig. 10). Using the BDFE calculated from eqn (1) and the square-scheme relationship, we can estimate the value for pK_{a2} to be ∼18, 7 pK_a units below the calculated pK_{a1} of 25.

The reactivity of **2** with 2,6-DTBP and DHA compares favorably with other reported high-valent metal–oxo and metal–hydroxo complexes capable of CPET or HAT (Table 1). **2** reacts with DHA at a faster rate than several manganese– and iron–oxo complexes. **2** also compares extremely well with high-valent metal alkoxide and carboxylate compounds, including the only other reported Ni(III) systems, which tend to react with C–H bonds at slower rates than their metal–oxo counterparts. We hypothesize that the particularly strong BDE of the ligand O–H bond formed and the strong oxidizing power of **2** contribute to its high reactivity toward O–H and C–H bonds. This result demonstrates that fast CPET can be achieved in high-valent metal systems without necessarily going through a metal–oxo or metal–hydroxo intermediate, a result relevant to several proposed water-oxidation mechanisms in artificial photosynthetic systems of cobalt,[49] copper,[11] and nickel.[50] This result also demonstrates that high-valent metal-alkoxide systems are capable of attacking strong C–H and O–H bonds, which is particularly relevant to water-oxidation catalysis. The pyalk ligand thus proves particularly useful for catalytic oxidations of this type.

Conclusions

We have synthesized and characterized a Ni(III)-alkoxide compound capable of reacting with strong C–H and O–H bonds at appreciable rates. A strong linear dependence between the second-order rate constant, k_2, and substrate bond dissociation enthalpy indicates a CPET mechanism. Large H/D kinetic isotope effects also support this assignment. We attribute the fast reactivity of **2** to the strong O–H BDE of the pyalk/pyalkH supporting ligand and the high oxidizing power of the complex. This result demonstrates that fast PCET can occur in high-valent metal oxidants without a metal–oxo unit, which may be relevant to certain nickel-containing enzymes or water-oxidation catalysts of cobalt, copper, or nickel. This report also provides the first full thermodynamic analysis of CPET by a high-valent nickel complex. The value of pyalk as a ligand for catalytic oxidations is further supported.

Conflicts of interest

There are no conflicts to declare.

Acknowledgements

This work was supported the U.S. Department of Energy, Office of Science, Office of Basic Energy Sciences, Division of Chemical Sciences, Geosciences, and Biosciences as part of the Center for Light Energy Activated Redox Processes (LEAP) Energy Frontier Research Center under Award Number DE-SC0001059. K. J. F. acknowledges the National Science Foundation Graduate Research Fellowship Program (Grant No. DGE1122492). We thank the Mass Spectrometry & Proteomics Resource and Dr Fabian Menges for assistance with HRMS. We would also like to thank Dr Min Li and Dr Liam Sharninghausen for collection of XPS data. We would also like to thank Professor Jim Mayer and Catherine Wise for their helpful comments.

References

1 B. Meunier, S. P. de Visser and S. Shaik, *Chem. Rev.*, 2004, **104**, 3947–3980.
2 P. R. Ortiz de Montellano and J. J. De Voss, *Nat. Prod. Rep.*, 2002, **19**, 477–493.
3 D. R. Weinberg, C. J. Gagliardi, J. F. Hull, C. F. Murphy, C. A. Kent, B. C. Westlake, A. Paul, D. H. Ess, D. G. McCafferty and T. J. Meyer, *Chem. Rev.*, 2012, **112**, 4016–4093.
4 Y. Zhang, H. Zhang, H. Ji, W. Ma, C. Chen and J. Zhao, *J. Am. Chem. Soc.*, 2016, **138**, 2705–2711.

5 D. C. Miller, K. T. Tarantino and R. R. Knowles, *Top. Curr. Chem.*, 2016, **374**, 30.
6 S. W. M. Crossley, C. Obradors, R. M. Martinez and R. A. Shenvi, *Chem. Rev.*, 2016, **116**, 8912–9000.
7 D. P. Barondeau, C. J. Kassmann, C. K. Bruns, J. A. Tainer and E. D. Getzoff, *Biochemistry*, 2004, **43**, 8038–8047.
8 J. Shearer, *Angew. Chem., Int. Ed.*, 2013, **52**, 2569–2572.
9 J. Shearer, *Acc. Chem. Res.*, 2014, **47**, 2332–2341.
10 T. K. Michaelos, D. Y. Shopov, S. B. Sinha, L. S. Sharninghausen, K. J. Fisher, H. M. C. Lant, R. H. Crabtree and G. W. Brudvig, *Acc. Chem. Res.*, 2017, **50**, 952–959.
11 B. Rudshteyn, K. J. Fisher, H. M. C. Lant, K. R. Yang, B. Q. Mercado, G. W. Brudvig, R. H. Crabtree and V. S. Batista, *ACS Catal.*, 2018, **8**, 7952–7960.
12 F. Chen, N. Wang, H. Lei, D. Guo, H. Liu, Z. Zhang, W. Zhang, W. Lai and R. Cao, *Inorg. Chem.*, 2017, **56**, 13368–13375.
13 P. Pirovano, E. R. Farquhar, M. Swart, A. J. Fitzpatrick, G. G. Morgan and A. R. McDonald, *Chem.–Eur. J.*, 2015, **21**, 3785–3790.
14 D. F. Evans and D. A. Jakubovic, *J. Chem. Soc., Dalton Trans.*, 1988, 2927–2933.
15 J. R. Lancaster, *The Bioinorganic Chemistry of Nickel*, VCH Publishers, 1988.
16 D. Y. Shopov, L. S. Sharninghausen, S. B. Sinha, B. Q. Mercado, D. Balcells, G. W. Brudvig and R. H. Crabtree, *Inorg. Chem.*, 2018, **57**, 5684–5691.
17 L. S. Sharninghausen, S. B. Sinha, D. Y. Shopov, B. Choi, B. Q. Mercado, X. Roy, D. Balcells, G. W. Brudvig and R. H. Crabtree, *J. Am. Chem. Soc.*, 2016, **138**, 15917–15926.
18 S. B. Sinha, D. Y. Shopov, L. S. Sharninghausen, C. J. Stein, B. Q. Mercado, D. Balcells, T. B. Pedersen, M. Reiher, G. W. Brudvig and R. H. Crabtree, *J. Am. Chem. Soc.*, 2017, **139**, 9672–9683.
19 L. S. Sharninghausen, S. B. Sinha, D. Y. Shopov, B. Q. Mercado, D. Balcells, G. W. Brudvig and R. H. Crabtree, *Angew. Chem.*, 2017, **129**, 13227–13231.
20 B. De Castro and C. Freire, *Inorg. Chem.*, 1990, **29**, 5113–5119.
21 P. Pirovano, E. R. Farquhar, M. Swart and A. R. McDonald, *J. Am. Chem. Soc.*, 2016, **138**, 14362–14370.
22 P. Mondal, P. Pirovano, A. Das, E. R. Farquhar and A. R. McDonald, *J. Am. Chem. Soc.*, 2018, **140**, 1834–1841.
23 K. J. Fisher, K. L. Materna, B. Q. Mercado, R. H. Crabtree and G. W. Brudvig, *ACS Catal.*, 2017, **7**, 3384–3387.
24 V. W. Manner, T. F. Markle, J. H. Freudenthal, J. P. Roth and J. M. Mayer, *Chem. Commun.*, 2008, 256–258.
25 T. H. Parsell, M.-Y. Yang and A. S. Borovik, *J. Am. Chem. Soc.*, 2009, **131**, 2762–2763.
26 R. Gupta and A. S. Borovik, *J. Am. Chem. Soc.*, 2003, **125**, 13234–13242.
27 B. Chiavarino, R. Cipollini, M. E. Crestoni, S. Fornarini, F. Lanucara and A. Lapi, *J. Am. Chem. Soc.*, 2008, **130**, 3208–3217.
28 T. Yoshida, K. Hirozumi, M. Harada, S. Hitaoka and H. Chuman, *J. Org. Chem.*, 2011, **76**, 4564–4570.
29 D. A. Pratt, G. A. DiLabio, P. Mulder and K. U. Ingold, *Acc. Chem. Res.*, 2004, **37**, 334–340.
30 D. Dhar, G. M. Yee, T. F. Markle, J. M. Mayer and W. B. Tolman, *Chem. Sci.*, 2017, **8**, 1075–1085.
31 D. E. Lansky and D. P. Goldberg, *Inorg. Chem.*, 2006, **45**, 5119–5125.
32 P. Mulder, O. W. Saastad and D. Griller, *J. Am. Chem. Soc.*, 1988, **110**, 4090–4092.
33 While the thermodynamics of this reaction are perhaps more accurately captured by the use of bond dissociation free energies (BDFEs), we chose to use BDEs in this analysis because of limited BDFE data for these compounds. A plot of $\log(k_2)$ *vs.* BDFE is provided in the ESI† for substrates with reported BDFEs.
34 D. Dhar and W. B. Tolman, *J. Am. Chem. Soc.*, 2015, **137**, 1322–1329.
35 J. R. Bryant and J. M. Mayer, *J. Am. Chem. Soc.*, 2003, **125**, 10351–10361.
36 J. W. Darcy, B. Koronkiewicz, G. A. Parada and J. M. Mayer, *Acc. Chem. Res.*, 2018, **51**, 2391–2399.
37 A. Kütt, S. Selberg, I. Kaljurand, S. Tshepelevitsh, A. Heering, A. Darnell, K. Kaupmees, M. Piirsalu and I. Leito, *Tetrahedron Lett.*, 2018, **59**, 3738–3748.
38 J. J. Warren, T. A. Tronic and J. M. Mayer, *Chem. Rev.*, 2010, **110**, 6961–7001.
39 T. R. Porter and J. M. Mayer, *Chem. Sci.*, 2014, **5**, 372–380.
40 M. H. Abraham, P. L. Grellier, D. V. Prior, R. W. Taft, J. J. Morris, P. J. Taylor, C. Laurence, M. Berthelot, R. M. Doherty, *et al.*, *J. Am. Chem. Soc.*, 1988, **110**, 8534–8536.
41 J. J. Warren and J. M. Mayer, *Proc. Natl. Acad. Sci. U. S. A.*, 2010, **107**, 5282.
42 Y. Gao, N. J. DeYonker, E. C. Garrett, A. K. Wilson, T. R. Cundari and P. Marshall, *J. Phys. Chem. A*, 2009, **113**, 6955–6963.
43 A. J. Johansson, M. R. A. Blomberg and P. E. M. Siegbahn, *J. Phys. Chem. C*, 2007, **111**, 12397–12406.
44 M. Finn, R. Friedline, N. K. Suleman, C. J. Wohl and J. M. Tanko, *J. Am. Chem. Soc.*, 2004, **126**, 7578–7584.
45 S. Kundu, E. Miceli, E. R. Farquhar and K. Ray, *Dalton Trans.*, 2014, **43**, 4264–4267.
46 C. R. Goldsmith, R. T. Jonas and T. D. P. Stack, *J. Am. Chem. Soc.*, 2002, **124**, 83–96.
47 B. A. Moyer and T. J. Meyer, *Inorg. Chem.*, 1981, **20**, 436–444.
48 E. L. Lebeau, R. A. Binstead and T. J. Meyer, *J. Am. Chem. Soc.*, 2001, **123**, 10535–10544.
49 D. Das, S. Pattanayak, K. K. Singh, B. Garai and S. Sen Gupta, *Chem. Commun.*, 2016, **52**, 11787–11790.
50 M. Zhang, M.-T. Zhang, C. Hou, Z.-F. Ke and T.-B. Lu, *Angew. Chem., Int. Ed.*, 2014, **53**, 13042–13048.

